JOURNAL OF MATERIALS SCIENCE 29 (1994) 4793–4801

Pull-out of a ductile fibre from a brittle matrix

Part I *Shear lag model*

CHUN-HWAY HSUEH
Metals and Ceramics Division, Oak Ridge National Laboratory, Oak Ridge, TN 37831, USA

Pull-out of a ductile fibre from a brittle matrix has been analysed using a shear lag model. Debonding at the fibre–matrix interface and yielding of the fibre occurred during the pull-out process. Both Poisson's contraction of the fibre and Coulomb friction of the debonded interface were considered. The debond length, which consists of an elastic zone length and a plastic zone length, was also analysed. When the fibre has a finite embedded length, it was found that necking prior to full pull-out of the fibre was required to optimize the toughening of a brittle matrix due to plastic deformation of the fibres. The essential material properties to achieve this are addressed.

1. Introduction

Brittle solids can be toughened by incorporating ductile inclusions. These inclusions can be particles [1–5], plates [6–9], or fibres [10–15]. Toughening of the brittle matrix is due to bridging of the crack surfaces by the ductile inclusions, and the toughening behaviour of the composite depends on the stress–displacement relation of the bridging inclusions. The present study was limited to fibres as the inclusions. In the presence of bonding at the fibre–matrix interface, the fibre is constrained and its stress–displacement curve is different from that of an unconstrained fibre [5, 10, 15]. Generally, the interface should not be very strong for optimum toughening. Strong (interfacial) bonding would result in a high degree of geometric constraint for the fibre, and the crack opening displacement corresponding to the fibre rupture would be very small which, in turn, results in a decrease in the toughening effect [5, 6, 9]. For long (or continuous) fibres, optimum toughening requires weak interfaces which result in extensive interfacial debonding to remove the constraint and to allow fibres to neck over extensive lengths until fracture [5, 9, 12]. However, when the fibre has a finite length, a critical minimum interfacial bond strength is required for optimum toughening. Otherwise, the fibre would be fully pulled out of the matrix before it necks which, in turn, minimizes both the crack-surface bridging action and the toughening effect [5, 9].

To analyse toughening of a brittle matrix by fibres, a single-fibre pull-out (i.e. the shear lag [16]) model has been adopted. When the fibre is brittle, the pull-out problem has been analysed extensively [17–25]. However, there exist only a few analyses for ductile fibres [9, 10, 12, 26]. The purpose of the present study was to extend the shear lag model to ductile fibre. Interfacial bonding, Coulomb friction at the debonded interface, and Poisson's contraction as well as elastic/plastic deformation of the fibre are considered in the present paper. First, the debond length, which consists of an elastic and a plastic zone lengths, during the pull-out process is analysed. Second, the distributions of the fibre axial stress and the interfacial shear stress along the debond length are presented. Third, effects of the interfacial bond strength, yield stress and strain-hardening rate of the (unconstrained) fibre, frictional coefficient and residual clamping stress at the debonded interface, and Young's modulus of the matrix on the (elastic/plastic) debond length are shown. Finally, for a finite fibre length, conditions of necking prior to pull-out of the fibre for optimum toughening are discussed.

2. The shear lag model

The shear lag model is depicted in Fig. 1. A ductile fibre with a radius, a, is embedded in a coaxial cylindrical shell of a brittle matrix with an outer radius, b. The radial and the axial coordinates are r and z, respectively. The fibre is subjected to an applied axial stress, σ_0, at the loaded surface, $z = h$, and the stress transfers from the fibre to the matrix through the interfacial shear stress, τ_i. In the present analysis, the following two conditions are assumed. (1) Interfacial debonding occurs prior to fibre yielding which is a premise for maximizing the toughening effect. (2) The interface is subjected to a residual clamping stress, σ_c, which, in turn, results in Coulomb friction upon interfacial debonding. This residual clamping can result from processing (i.e. densification shrinkage of the ceramic matrix against the already dense fibre), thermomechanical mismatch between the fibre and the matrix during cooling from the fabrication temperature, or the asperities along the interface. In the presence of interfacial asperities, an interfacial compressive stress is induced as the fibre attempts to slide past the matrix [12, 23, 27–29].

Fig. 1 shows that (1) the interface debonds along a length, h, such that the end of the debond zone is located at $z = 0$, (2) the fibre yields along a length, $h - h_y$, such that the end of the plastic zone is located at $z = h_y$, and (3) at the end of the debond zone, the

0022–2461

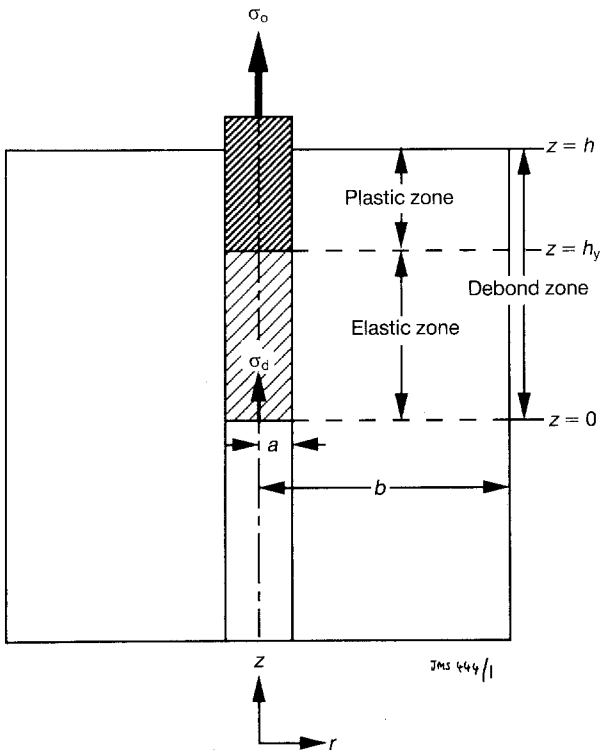

Figure 1 Schematic illustration of the shear-lag model used in analysing pull-out of a ductile fibre from a brittle matrix. The debond length, h, which consists of an elastic and a plastic zone lengths (h_y and $h - h_y$), is also shown.

axial stress in the fibre is in equilibrium with the bond strength, σ_d. This bond strength can be related to the interfacial shear strength or the interfacial fracture energy depending on whether the strength-based [17, 18, 25] or the energy-based [21, 30, 31] debonding criterion is used. With given material properties, both h and h_y are functions of σ_0.

For the shear lag model, the differential equation governing the axial stress distribution in the fibre, σ_f, during fibre pull-out has been derived, such that [25]

$$\frac{d^2\sigma_f}{dz^2} = \left[\sigma_f - \sigma_0 + \left(\frac{b^2}{a^2} - 1\right)\sigma_a\right] \Big/ (1 + \nu_m)\left[\frac{b^4}{b^2 - a^2}\ln\left(\frac{b}{a}\right) - \frac{3b^2 - a^2}{4}\right] \quad (1)$$

where ν_m is Poisson's ratio of the matrix, and σ_a is the axial stress in the matrix at $r = a$. The solution of σ_f is contingent upon the determination of σ_a. Depending upon the characteristic of the interface (i.e. bonded or debonded) and the mechanical behaviour of the material (i.e. elastic or plastic), σ_a can be determined accordingly. For a bonded interface, the solutions have been obtained previously when the fibre remains elastic [24, 25]. Interfacial debonding prior to fibre yielding is considered in the present study. The solutions after debonding and prior to yielding are presented in Section 3, and the solutions after yielding and prior to necking are presented in Section 4. After necking, the strain is restricted to the necked region, the stress–strain curve of the fibre depends on the cavitation process in the necked region and is beyond the scope of the present study.

3. Elastic solutions (prior to yielding)

When the fibre remains elastic during the pull-out process, the solutions have been obtained previously [24]. However, a deficiency exists in the existing solutions, i.e. the shear stress at $r = b$ satisfies the free surface condition only approximately [24]. Modifications of the analyses to satisfy this free surface condition have been addressed [25]. Without repeating the analyses, the solutions, which satisfy the free surface condition at $r = b$, are listed in the present study.

The relation between the applied stress and the sliding length (i.e. σ_0 versus h) is given by Equation A3 in [32]. The fibre axial stress, σ_f, and the interfacial shear stress, τ_i, along the sliding length are given by Equations 8 and A19 in [33]. However, to satisfy the free surface condition at $r = b$, the parameters A_1, A_2, and A_3 in the above equations should be replaced by

$$A_1 = a\left(1 - \frac{b^2}{a^2}\right)D \Big/ 2\mu\nu_m(1 + \nu_m)\left[\frac{b^4}{b^2 - a^2}\ln\left(\frac{b}{a}\right) - \frac{3b^2 - a^2}{4}\right] \quad (2a)$$

$$A_2 = \left[\left(1 - \frac{b^2}{a^2}\right)\frac{E_m\nu_f}{E_f\nu_m} - 1\right] \Big/ (1 + \nu_m)\left[\frac{b^4}{b^2 - a^2}\ln\left(\frac{b}{a}\right) - \frac{3b^2 - a^2}{4}\right] \quad (2b)$$

$$A_3 = \left[-\sigma_0 - \left(1 - \frac{b^2}{a^2}\right)\frac{D\sigma_c}{\nu_m}\right] \Big/ (1 + \nu_m)\left[\frac{b^4}{b^2 - a^2}\ln\left(\frac{b}{a}\right) - \frac{3b^2 - a^2}{4}\right] \quad (2c)$$

where E and ν are Young's modulus and Poisson's ratio, the subscripts f and m denote the fibre and the matrix, μ is the coefficient of friction at the interface and D is given by

$$D = \frac{b^2 + a^2}{b^2 - a^2} + \nu_m + \frac{E_m(1 - \nu_f)}{E_f} \quad (3)$$

4. Elastic/plastic solutions (after yielding)

During the pull-out process, an interfacial radial stress, σ_p, is induced due to Poisson's effect. For a frictional interface, the axial stresses in the fibre and the matrix, σ_f and σ_m, vary slowly over distances comparable to the fibre radius. In this case, the radial and the tangential stresses, σ_r and σ_θ, can be related to σ_p by [21, 32]

$$\sigma_{fr} = \sigma_{f\theta} = \sigma_p \quad (4)$$

for the fibre, and [21, 32]

$$\sigma_{mr} = \sigma_p \quad \text{at } r = a \quad (5a)$$

$$\sigma_{m\theta} = \frac{-(b^2 + a^2)\sigma_p}{b^2 - a^2} \quad \text{at } r = a \quad (5b)$$

for the matrix at the interface.

The stress transfer from the fibre to the matrix, and the Coulomb friction at the interface are dictated by

$$\frac{d\sigma_f}{dz} = -\frac{2\tau_i}{a} \tag{6}$$

$$\tau_i = \mu(\sigma_c + \sigma_p). \tag{7}$$

The condition that the fibre and the matrix remain in contact during frictional sliding requires continuity of the tangential strain at the interface. Depending upon the mechanical behaviour of the fibre (i.e. plastic or elastic), the corresponding analyses are performed, respectively, in Sections 4.1 and 4.2.

4.1. The plastic zone ($h \geqslant z \geqslant h_y$)

With the residual clamping stress, σ_c, and the induced interfacial radial stress, σ_p, due to Poisson's effect, the radial constraint of the fibre is $\sigma_c + \sigma_p$. Using the Von Mises yield criterion [34], assuming the plastic strain satisfying the Prandtl–Reuss relation [34], and assuming linear strain-hardening, the plastic strains ε_z^p, ε_r^p and ε_θ^p in the fibre are (see Equations 5–12 in [35])

$$\varepsilon_z^p = \frac{\sigma_f - \sigma_c - \sigma_p - \sigma_y}{H} \tag{8a}$$

$$\varepsilon_r^p = \varepsilon_\theta^p = -\frac{\sigma_f - \sigma_c - \sigma_p - \sigma_y}{2H} \tag{8b}$$

where H is the slope of the strain-hardening curve, and σ_y is the yield stress of the unconstrained fibre. Hence, the yield stress of the constrained fibre, which is subjected to triaxial stresses, becomes $\sigma_c + \sigma_p + \sigma_y$.

The fibre/matrix system subjected to the residual stress is in mechanical equilibrium prior to loading. During loading, continuity of the tangential strain at the interface requires

$$\frac{(1-\nu_f)\sigma_p - \nu_f\sigma_f}{E_f} - \frac{\sigma_f - \sigma_c - \sigma_p - \sigma_y}{2H} = \left[-\left(\frac{b^2+a^2}{b^2-a^2} + \nu_m\right)\sigma_p - \nu_m\sigma_a\right] \Big/ E_m \tag{9}$$

Combination of Equations 6, 7 and 9 yields

$$\sigma_a = \frac{1}{\nu_m}\left[\frac{a}{2\mu}\left(D + \frac{E_m}{2H}\right)\frac{d\sigma_f}{dz} + \left(\frac{E_m\nu_f}{E_f} + \frac{E_m}{2H}\right)\sigma_f + D\sigma_c - \frac{E_m\sigma_y}{2H}\right] \tag{10}$$

Substitution of σ_a into Equation 1 yields

$$\frac{d^2\sigma_f}{dz^2} + B_1\frac{d\sigma_f}{dz} + B_2\sigma_f = B_3 \tag{11}$$

where

$$B_1 = a\left(1 - \frac{b^2}{a^2}\right)\left(D + \frac{E_m}{2H}\right) \Big/ 2\mu\nu_m(1+\nu_m) \times \left[\frac{b^4}{b^2-a^2}\ln\left(\frac{b}{a}\right) - \frac{3b^2-a^2}{4}\right] \tag{12a}$$

$$B_2 = \left[\left(1 - \frac{b^2}{a^2}\right)\frac{E_m}{\nu_m}\left(\frac{\nu_f}{E_f} + \frac{1}{2H}\right) - 1\right] \Big/ (1+\nu_m)\left[\frac{b^4}{b^2-a^2}\ln\left(\frac{b}{a}\right) - \frac{3b^2-a^2}{4}\right] \tag{12b}$$

$$B_3 = \left[-\sigma_0 - \left(1 - \frac{b^2}{a^2}\right)\frac{1}{\nu_m}\left(D\sigma_c - \frac{E_m\sigma_y}{2H}\right)\right] \Big/ (1+\nu_m)\left[\frac{b^4}{b^2-a^2}\ln\left(\frac{b}{a}\right) - \frac{3b^2-a^2}{4}\right] \tag{12c}$$

The solution of σ_f is subjected to the following two boundary conditions. First, the axial stress in the fibre is in equilibrium with the applied stress at the loaded surface, such that

$$\sigma_f = \sigma_0 \quad \text{at } z = h \tag{13a}$$

Second, the plastic strain is zero at the end of the plastic zone, such that

$$\sigma_f = \sigma_c + \sigma_p + \sigma_y \quad \text{at } z = h_y \tag{13b}$$

The solution of Equation 11 subjected to the above boundary conditions is

$$\sigma_f = \frac{B_3}{B_2}\{1 - \exp[n_2(z-h)]\} + C\{\exp(n_1 z) - \exp[n_1 h + n_2(z-h)]\} + \sigma_0\exp[n_2(z-h)] \tag{14}$$

where

$$C = [\sigma_y - [1 + (an_2/2\mu)]\exp[n_2(h_y - h)]\sigma_0 - (B_3/B_2)\{1 - [1 + (an_2/2\mu)]\exp[n_2(h_y - h)]\}] / \{1 + (an_1/2\mu)]\exp(n_1 h_y) - [(1 + (an_2/2\mu)] \times \exp[n_1 h + n_2(h_y - h)]\} \tag{15a}$$

$$n_1 = \frac{-B_1 + (B_1^2 - 4B_2)^{1/2}}{2} \tag{15b}$$

$$n_2 = \frac{-B_1 - (B_1^2 - 4B_2)^{1/2}}{2} \tag{15c}$$

The corresponding interfacial shear stress can be obtained from Equations 6 and 14.

The complete solutions are contingent upon the solutions of both h and h_y. These can be achieved by satisfying (1) continuity conditions at the elastic/plastic boundary (i.e. at $z = h_y$), and (2) the free surface condition for the matrix at $z = h$. While the first condition requires the solutions in the elastic zone (which will be solved in Section 4.2), the second condition leads to

$$\sigma_0 = \left(P_1\left\{\left(\frac{b^2}{a^2} - 1\right)\frac{P_2}{\nu_m}\left(D\sigma_c - \frac{E_m\sigma_y}{2H}\right) + (n_1 - n_2) \times \exp[(n_1 + n_2)(h - h_y)]\sigma_y\right\} + D\sigma_c - \frac{E_m\sigma_y}{2H}\right) \Big/ \left[P_1\left\{P_2 + n_1\left(1 + \frac{an_2}{2\mu}\right)\exp[n_1(h - h_y)] - n_2\left(1 + \frac{an_1}{2\mu}\right)\exp[n_2(h - h_y)]\right\} - E_m\left(\frac{\nu_f}{E_f} + \frac{1}{2H}\right)\right] \tag{16}$$

where

$$P_1 = \frac{a}{2\mu}\left(D + \frac{E_m}{2H}\right)\Big/\left[\left(1 + \frac{an_1}{2\mu}\right)\exp[n_2(h - h_y)] - \left(1 + \frac{an_2}{2\mu}\right)\exp[n_1(h - h_y)]\right] \quad (17a)$$

$$P_2 = \Big\{-(n_1 - n_2)\exp[(n_1 + n_2)(h - h_y)] + n_1\left(1 + \frac{an_2}{2\mu}\right)\exp[n_1(h - h_y)] - n_2\left(1 + \frac{an_1}{2\mu}\right)\exp[n_2(h - h_y)]\Big\}\Big/\left[\left(1 - \frac{b^2}{a^2}\right)\frac{E_m}{\nu_m}\left(\frac{\nu_f}{E_f} + \frac{1}{2H}\right) - 1\right] \quad (17b)$$

4.2. The elastic zone ($h_y \geqslant z \geqslant 0$)

Without the plastic strain component in Equation 9, σ_a becomes

$$\sigma_a = \frac{1}{\nu_m}\left[D\left(\sigma_c + \frac{a}{2\mu}\frac{d\sigma_f}{dz}\right) + \frac{E_m\nu_f\sigma_f}{E_f}\right] \quad (18)$$

Substitution of σ_a into Equation 1 yields

$$\frac{d^2\sigma_f}{dz^2} + A_1\frac{d\sigma_f}{dz} + A_2\sigma_f = A_3 \quad (19)$$

where A_1, A_2, and A_3 are given by Equations 2a–c. The solution of σ_f is subjected to the following two boundary conditions. First, the axial stress in the fibre is in equilibrium with the bond strength at the end of the debond zone, such that

$$\sigma_f = \sigma_d \qquad \text{at } z = 0 \quad (20a)$$

Second, σ_f is continuous at $z = h_y$, such that

$$\sigma_f = \sigma_c + \sigma_p + \sigma_y \qquad \text{at } z = h_y \quad (20b)$$

The solution of Equation 19 subjected to the above boundary conditions is

$$\sigma_f = \frac{A_3}{A_2}[1 - \exp(m_2 z)] + B[\exp(m_1 z) - \exp(m_2 z)] + \sigma_d\exp(m_2 z) \quad (21)$$

where

$$B = \Big\{\sigma_y - \left(1 + \frac{am_2}{2\mu}\right)\exp(m_2 h_y)\sigma_d - \frac{A_3}{A_2}\left[1 - \left(1 + \frac{am_2}{2\mu}\right)\exp(m_2 h_y)\right]\Big\}\Big/\left[\left(1 + \frac{am_1}{2\mu}\right)\exp(m_1 h_y) - \left(1 + \frac{am_2}{2\mu}\right)\exp(m_2 h_y)\right] \quad (22a)$$

$$m_1 = \frac{-A_1 + (A_1^2 - 4A_2)^{1/2}}{2} \quad (22b)$$

$$m_2 = \frac{-A_1 - (A_1^2 - 4A_2)^{1/2}}{2} \quad (22c)$$

The corresponding interfacial shear stress can be obtained from Equations 6 and 21.

The complete solution of σ_f (Equation 21) is contingent upon the solution of h_y, which is solved as follows. Continuities of the axial stress in the matrix and of the interfacial shear stress at $z = h_y$ are required. It was found that these continuity conditions are fulfilled by continuity of σ_a at $z = h_y$. Equating Equation 10 to Equation 18 at $z = h_y$, the result is

$$\sigma_0 = \Big\{\left(1 - \frac{b^2}{a^2}\right)\frac{(R_1 - Q_1)D\sigma_c}{\nu_m} + \left[R_2 - Q_2 + \left(1 - \frac{b^2}{a^2}\right)\frac{Q_1 E_m}{2\nu_m H}\right]\sigma_y + \left[m_2 - R_2\left(1 + \frac{am_2}{2\mu}\right)\right]\exp(m_2 h_y)\sigma_d\Big\}\Big/\Big\{Q_1 - R_1 + \left[n_2 - Q_2\left(1 + \frac{an_2}{2\mu}\right)\right] \times \exp[n_2(h_y - h)]\Big\} \quad (23)$$

where

$$Q_2 = \{n_1\exp[n_2(h - h_y)] - n_2\exp[n_1(h - h_y)]\}\Big/\Big\{\left(1 + \frac{an_1}{2\mu}\right)\exp[n_2(h - h_y)] - \left(1 + \frac{an_2}{2\mu}\right) \times \exp[n_1(h - h_y)]\Big\} \quad (24a)$$

$$Q_1 = \left(n_2 + Q_2\left\{\exp[n_2(h - h_y)] - \left(1 + \frac{an_2}{2\mu}\right)\right\}\right)\Big/\Big\{\left[\left(1 - \frac{b^2}{a^2}\right)\frac{E_m}{\nu_m}\left(\frac{\nu_f}{E_f} + \frac{1}{2H}\right) - 1\right] \times \exp[n_2(h - h_y)]\Big\} \quad (24b)$$

$$R_2 = [m_1\exp(m_1 h_y) - m_2\exp(m_2 h_y)]\Big/\left[\left(1 + \frac{am_1}{2\mu}\right) \times \exp(m_1 h_y) - \left(1 + \frac{am_2}{2\mu}\right)\exp(m_2 h_y)\right] \quad (24c)$$

$$R_1 = \Big\{m_2\exp(m_2 h_y) + R_2\left[1 - \left(1 + \frac{am_2}{2\mu}\right) \times \exp(m_2 h_y)\right]\Big\}\Big/\left[\left(1 - \frac{b^2}{a^2}\right)\frac{E_m\nu_f}{E_f\nu_m} - 1\right] \quad (24d)$$

For a given σ_0, solutions of h and h_y can be obtained by satisfying Equations 16 and 23 simultaneously, which require numerical analyses.

5. Results

The properties of W–3Re fibre-reinforced TiTaAl composites [15] are used for the present analyses. The reported properties are $E_f = 350$ GPa, $E_m = 190$ GPa, $\nu_f = 0.28$, $\nu_m = 0.23$, $\sigma_y = 1.9$ GPa, $\sigma_d = 80$ MPa, $a = 37.5$ μm, and the volume fraction of fibres is 0.16 [15]. The thermal expansion coefficients are $\alpha_f = 4.5 \times 10^{-6}\,K^{-1}$ and $\alpha_m = 10 \times 10^{-6}\,K^{-1}$, and the

cooling temperature is -1180 K [15]. Assuming that the residual interfacial clamping stress, σ_c, is due to thermal mismatch during cooling, the calculated σ_c using the analyses in [36] is -823.5 MPa. In the shear lag model, the material surrounding the fibre is treated as the matrix. Owing to the high volume fraction of fibres, the rule of mixtures is used to estimate the elastic properties for the matrix (i.e. $E_m = 215.6$ GPa, $\nu_m = 0.238$) in the shear lag model. It was found that the calculated results are insensitive to b/a when $b/a \geqslant 10$. Hence, $b/a = 10$ is used in the present calculation.

Unless noted otherwise, the above properties, $\mu = 0.2$, and $H = 250$ GPa are used in the present calculation to elucidate the essential trends. First, an example of determining the debond length, h, and the plastic zone length, $h - h_y$, during the pull-out process is illustrated. Second, an example of distributions of the axial stress in the fibre and the interfacial shear stress along the debond length is given. Third, the effects of σ_d, σ_y, H, μ, σ_c, and E_m on both h and $h - h_y$ are examined. Finally, when the embedded fibre length is finite, the conditions for necking prior to pull-out of the fibre are presented.

5.1. Determination of the debond length and the plastic zone length

Interfacial debonding initiates when the applied stress, σ_0, reaches the interfacial bond strength, σ_d, The debond length increases without plastic deformation of the fibre with increasing σ_0 until σ_0 reaches $\sigma_c + \sigma_p + \sigma_y$, where σ_p is a function of σ_0. At this point, plastic deformation develops, and both the debond length and the plastic zone length increase with increasing σ_0 which are determined as follows.

In the absence of plastic deformation, the closed-form analytical solution for the applied stress–debond length relation is given in Section 3. Plotting both σ_0 and $\sigma_c + \sigma_p + \sigma_y$ versus the debond length curves, the applied stress and the debond length at which plastic deformation initiates can be obtained from the intersection of these two curves (Fig. 2). Compared to the yield stress of the unconstrained fibre (i.e. 1.9 GPa), the calculated yield stress of the constrained fibre is 0.7 GPa lower (i.e. 1.2 GPa) which is in good agreement with the measurement (~ 1.3 GPa [15]). This decrease of the tensile yield stress for the constrained fibre was earlier interpreted to be a result of the existence of the residual tensile axial stress in the matrix in [15]. In the present study, this decrease is due to the fact that the constrained fibre is subjected to triaxial stresses, in which a strong interfacial residual clamping contributes to this decrease.

In the presence of plastic deformation, the debond length, h, consists of an elastic zone length, h_y, and a plastic zone length, $h - h_y$ (see Fig. 1). During the pull-out process, h increases; however, it was found in the present calculation that the elastic zone length, h_y, shows a slight decrease after yielding. This slight decrease in h_y is due to the change in σ_m at $z = h_y$ during the pull-out process. For a fixed h_y, which is slightly smaller than the debond length at which plastic deformation initiates, the σ_0 versus $h - h_y$ curves are plotted using Equation 16 and 23, respectively. While equation 16 is a function of $h - h_y$ and is independent of h_y, Equation 23 is a function of both $h - h_y$ and h_y. For a given h_y, the applied stress, the plastic zone length, and the debond length can be obtained from intersection of these two curves (Fig. 3a). This process is repeated for different values of h_y (see Fig. 3a), and both the debond length and the plastic zone length versus the applied stress relations are obtained as shown in Fig. 3b. The debond length versus the applied stress relation prior to yielding is also shown (Fig. 3b). After yielding, the slight decrease in h_y during pull-out can be seen in Fig. 3a. For example, when σ_0 increases from ~ 2.1 GPa to ~ 2.35 GPa, h_y/a decreases from 3.727 to 3.724 while $(h - h_y)/a$ increases from ~ 4 to ~ 5.6.

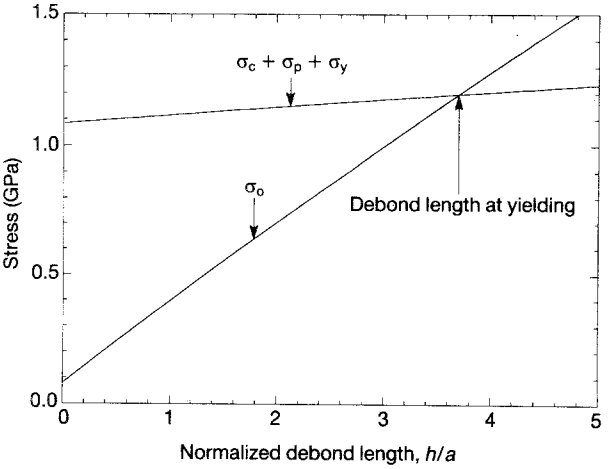

Figure 2 The σ_0 and $\sigma_c + \sigma_p + \sigma_y$ versus the normalized debond length h/a relations for determining the applied stress and the debond length at which yielding occurs.

5.2. The stress distribution

The distributions of the axial stress in the fibre, σ_f, and the interfacial shear stress, τ_i, along the debond length are shown in Fig. 4 for $\sigma_0 = 2.038$ GPa. The axial stress in the fibre is the applied stress at the loaded surface, and decreases non-linearly to the bond strength at the end of the debond length ($z = 0$). The interfacial shear stress has the smallest magnitude at the loaded surface due to Poisson's effect. Both σ_f and τ_i are continuous at the elastic/plastic boundary ($z = h_y$). However, owing to the presence of plasticity in the plastic zone, the slope of the $\tau_i - z$ curve changes at the elastic/plastic boundary.

5.3. Effects of σ_d, σ_y, H, μ, σ_c, and E_m

The effects of the parameters, σ_d, σ_y, H, μ, σ_c, and E_m, on the debond length, h, and the plastic zone length, $h - h_y$, are obtained by changing these parameters, arbitrarily, one at a time. It is noted that before yielding, the elastic zone length, h_y, increases with increasing applied stress, σ_0. After yielding, h_y shows a slight decrease with increasing σ_0. This slight decrease in h_y (h_y decreases by $\sim 0.03a$ when σ_0 increases from

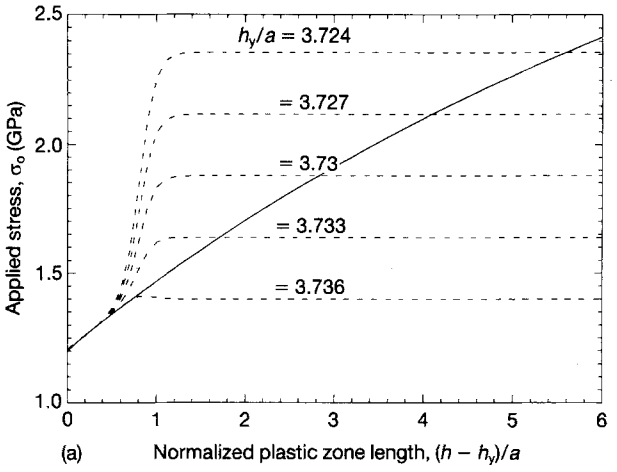

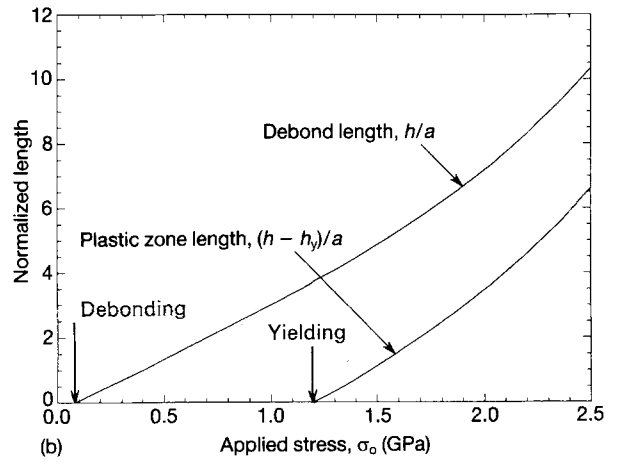

Figure 3 (a) For given elastic zone lengths, h_y, the stress versus the plastic zone length (σ_0 versus $h - h_y$) relations are plotted based on Equations (——) 16 and (– – –) 23 to determine the plastic zone length. (b) The debond length, h, and the plastic zone length, $h - h_y$, as functions of the applied stress.

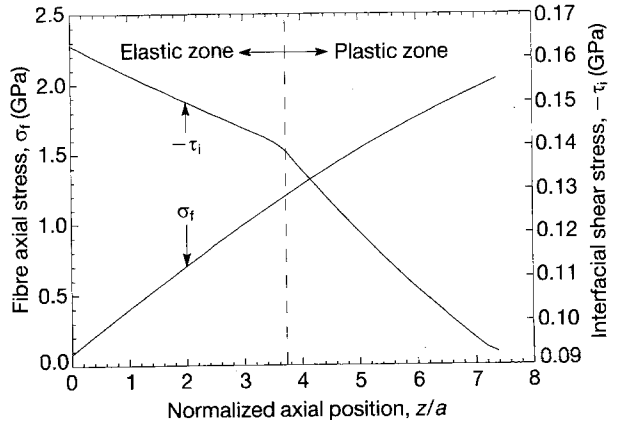

Figure 4 The axial stress in the fibre, σ_f, and the interfacial shear stress, $-\tau_i$, as functions of the normalized axial position, z/a, for $\sigma_0 = 2.038$ GPa.

~ 1.2 GPa, the yield stress of the constrained fibre, to 2.5 GPa) is ignored in the present discussion. The effects of these parameters are shown in Fig. 5a–f, and are discussed as follows.

Fig. 5a shows that interfacial debonding occurs at a higher stress when the bond strength, σ_d, increases. Both the debond length and the elastic zone length decrease, but the plastic zone length remains unchanged with increasing σ_d (at the same σ_0) (Fig. 5a). Fig. 5b shows that the constrained fibre yields at a lower stress when the yield stress of the unconstrained fibre, σ_y, decreases. After yielding, both the debond length and the plastic zone length increase, but the elastic zone length, h_y, decreases with decreasing σ_y (Fig. 5b). This decrease in h_y is due to the earlier development of yielding with decreasing σ_y which, in turn, limits the development of the elastic zone. When strain-hardening rate, H, decreases, the plastic zone length increases and the elastic zone length remains the same (Fig. 5c).

When the coefficient of friction, μ, increases, both the elastic and the plastic zone lengths decrease (Fig. 5d) due to the increase in the frictional resistance at the debonded interface. When the magnitude of the residual clamping stress, σ_c, decreases, both the debond length and the elastic zone length increase (due to the decreasing frictional resistance), and although yielding initiates at a higher stress, the plastic zone length increases when the load is sufficiently high (due to the decreasing frictional resistance) (Fig. 5e). This increase in the yield stress of the constrained fibre with the decreasing magnitude of the residual clamping stress is due to the constrained fibre yielding at a stress of $\sigma_c + \sigma_p + \sigma_y$, where σ_c is negative (i.e. compressive).

When the Young's modulus of the matrix, E_m, is decreased, both the debond length and the elastic zone length decrease, and although yielding initiates at a lower stress, the plastic zone length decreases when the load is sufficiently high (Fig. 5f). The interfacial radial stress induced due to Poisson's effect, σ_p (tensile and positive), decreases with decreasing E_m which, in turn, results in increasing frictional resistance and a decreasing yield stress for the constrained fibre.

5.4. The conditions for necking prior to pull-out of the fibre

After yielding, an unconstrained ductile fibre deforms with a uniform axial strain along the length. When this uniform axial strain reaches a critical value, necking occurs and the load support capacity of the fibre drops. The uniform axial strain, ε_z, in the *unconstrained* fibre is

$$\varepsilon_z = \frac{\sigma_0}{E_f} + \frac{\sigma_0 - \sigma_y}{H} \tag{25}$$

Owing to the stress transfer between the fibre and the matrix, a *constrained* fibre has a non-uniform axial strain distribution along the fibre length prior to necking. It is assumed in the present study that necking of the constrained fibre occurs when the maximum axial strain ε_{z0}, which occurs at the loaded surface ($z = h$), in the fibre reaches a critical value. Considering the strain due to both the loading and the residual clamping stress, ε_{z0} is

$$\varepsilon_{z0} = \frac{\sigma_0 - 2\nu_f(\sigma_c + \sigma_p)}{E_f} + \frac{\sigma_0 - \sigma_c - \sigma_p - \sigma_y}{H} \quad \text{at } z = h \tag{26}$$

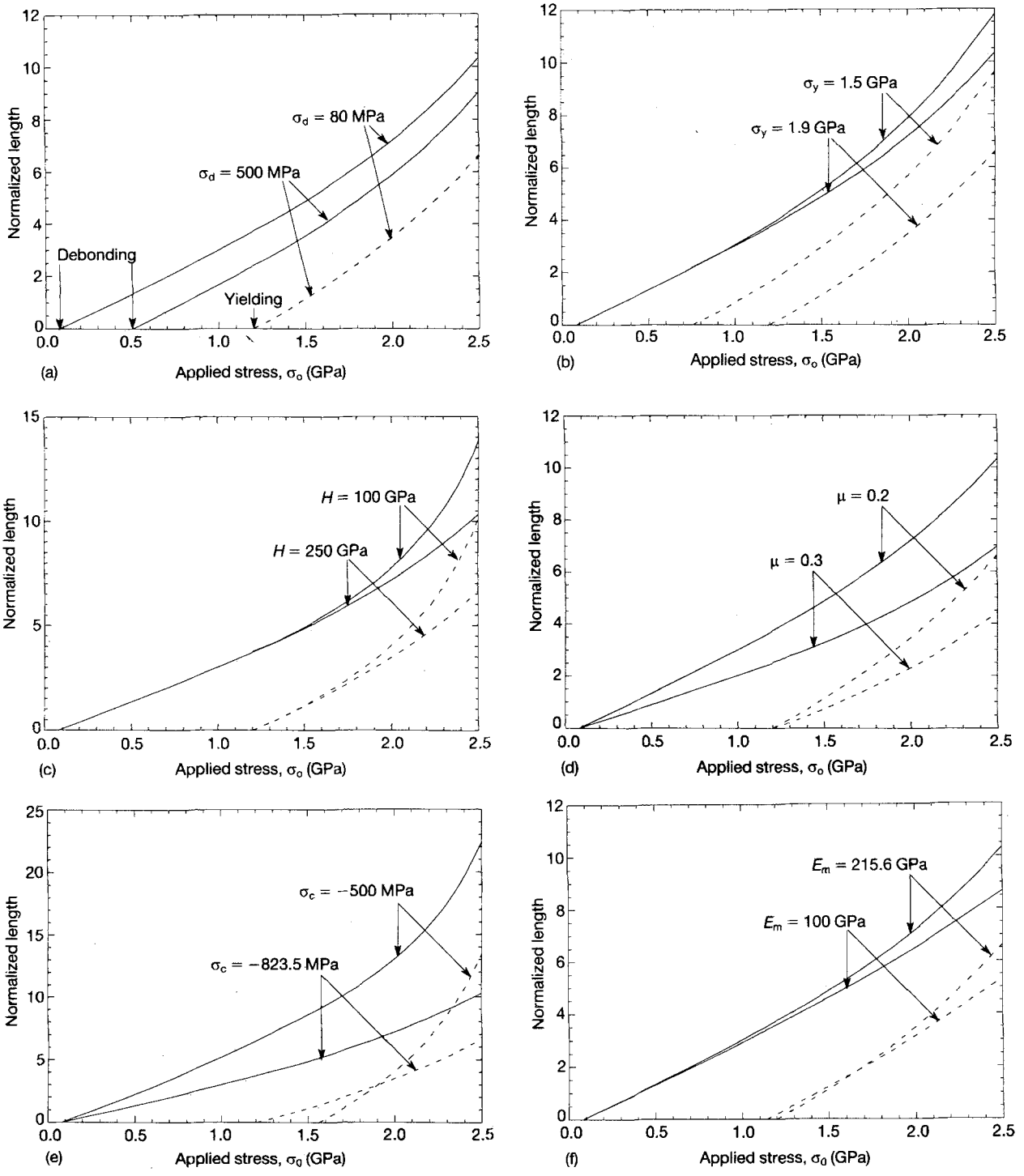

Figure 5 Effects of (a) bond strength, σ_d, (b) yield stress, σ_y, (c) strain-hardening rate, H, (d) frictional coefficient, μ, (e) residual clamping stress, σ_c, and (f) Young's modulus of the matrix, E_m, on (——) the debond length, h, and (– – –) the plastic zone length, $h - h_y$.

The reported ultimate strengths of the unconstrained and constrained W–3Re fibres are ~ 2.9 and ~ 2.5 GPa, respectively [15]. Using the material properties listed in Section 5, the calculated critical axial strains for the unconstrained (Equation 25) and the constrained (Equation 26) fibres are both ~ 1.2%. Hence, the adoption of H = 250 GPa in the present calculation yields consistent results in the critical strain for necking between the unconstrained and the constrained fibres. The measured failure strain is ~ 3% [15], but the measured critical strain for necking is unavailable. However, if the measured critical strain and strain-hardening are available, the parameters used in the present calculation can be adjusted accordingly.

Assuming that the critical strain for necking is 1.2%, the condition for necking requires that the maximum axial strain in the fibre reaches 1.2% before the debond length reaches the end of the embedded fibre. When the fibre has a finite length, with other parameters fixed, the requirements of the bond strength, σ_d, and the yield stress, σ_y, for necking to occur are analysed, respectively, in this section. First, both the debond length and the plastic zone length are plotted as functions of the maximum axial strain in the fibre, ε_{z0}, at different values of the bond strength (Fig. 6a).

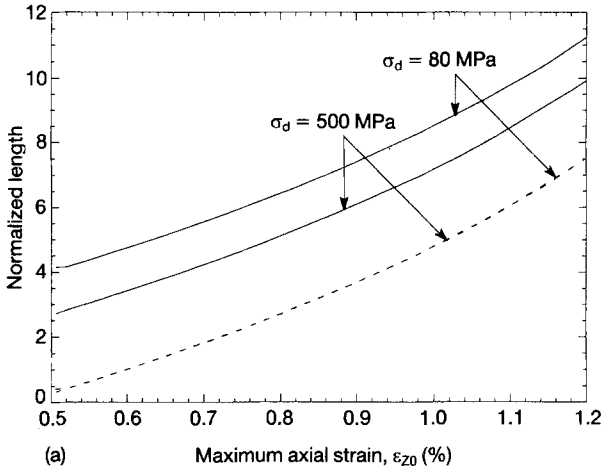

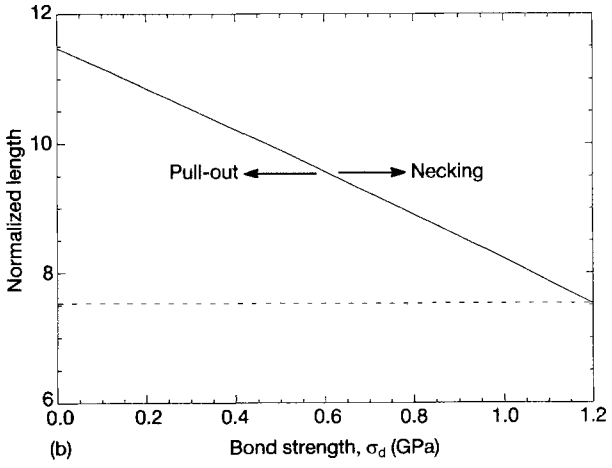

Figure 6 (a) The (——) debond length, h, and (– – –) the plastic zone length, $h - h_y$, as functions of the maximum axial strain at different values of the bond strength, σ_d. (b) The debond length, h, and the plastic zone length, $h - h_y$, as functions of the bond strength, σ_d, when the critical axial strain for necking is 1.2%.

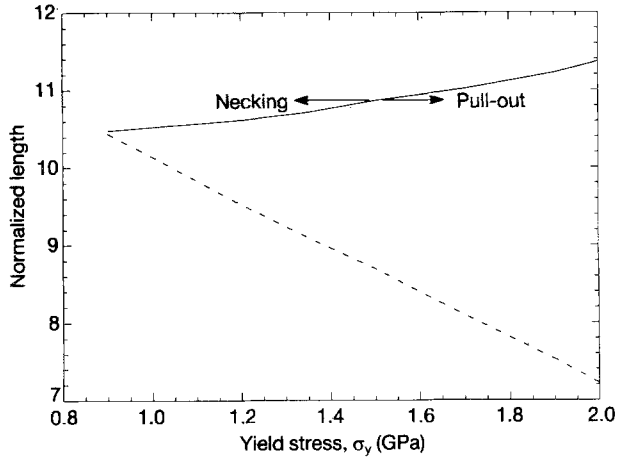

Figure 7 (——) The debond length, h, and (– – –) the plastic zone length, $h - h_y$, as functions of the yield stress, σ_y, when the critical axial strain for necking is 1.2%.

Then, at $\varepsilon_{z0} = 1.2\%$, both the debond length and the plastic zone length obtained from Fig. 6a are plotted as functions of the bond strength (Fig. 6b). Fig. 6b shows that the plastic zone length which develops prior to necking is independent of the bond strength; however, the debond length decreases with the increasing bond strength. Hence, for a given embedded fibre length, necking of the fibre requires that the bond strength is greater than a critical value (Fig. 6b).

Using the same procedure, the requirements of σ_y for necking are plotted in Fig. 7. Prior to necking, the plastic zone length decreases and the debond length increases with increasing σ_y. Hence, for a given embedded fibre length, necking of the fibre requires that the yield stress is smaller than a critical maximum value. However, σ_y should also be greater than a critical minimum value ($\sim$ 0.9 GPa in Fig. 7) to ensure that debonding occurs prior to yielding. It is noted that the debond length, h, decreases with increasing σ_y at fixed σ_0 (Fig. 5b), but h increases with increasing σ_y at fixed ε_{z0} (Fig. 7). This is due to ε_{z0} reaching 1.2% at a higher σ_0 when σ_y has a higher value.

6. Conclusion

Optimum toughening of a brittle matrix by ductile fibres requires that interfacial debonding occurs before yielding of the fibre during the fibre pull-out process. Furthermore, when the fibre has a finite embedded length, necking prior to its full pull-out is required. To examine the toughening condition, pull-out of a ductile fibre from a brittle matrix is analysed in the present study. When the fibre is constrained (i.e. embedded in matrix), the yield stress is modified due to the presence of triaxial stresses. Specifically, the tensile yield stress of a constrained fibre decreases when (1) the yield stress of the unconstrained fibre decreases, (2) the magnitude of the residual clamping stress increases, or (3) the Young's modulus of the matrix decreases.

When the yield stress of a constrained fibre is greater than the bond strength, interfacial debonding occurs during the pull-out process. The debond length increases with increasing applied stress until the fibre yields. Then with further loading, both the debond length (which consists of an elastic and a plastic zone lengths) and the plastic zone length increase; however, the elastic zone length shows a negligible decrease. When the maximum axial strain, which occurs at the loaded surface, in the fibre reaches a critical value, necking initiates. However, when the fibre has a finite embedded length, the maximum axial strain should reach the critical strain for necking before the debond length reaches the embedded length to ensure necking of the fibre.

The effects of the bond strength, the yield stress, the strain-hardening rate, the frictional coefficient at the debonded interface, the residual clamping stress at the interface, and the Young's modulus of the matrix on the debond length, the plastic zone length, and the elastic zone length are examined in Fig. 5a–f. When the fibre has a finite embedded length, the plastic zone length should be maximized while the elastic zone length should be minimized during the pull-out process to utilize plastic deformation of the fibre as the toughening mechanism. Among the parameters discussed in the present study, this is best achieved by having the bond strength smaller but close to the yield stress of the constrained fibre.

The present analysis is applicable when the debonded interface is subjected to Coulomb friction. The present solutions offer the conditions for the interface to debond, and for the fibre to yield and to neck. After necking, the stress–strain relation of the fibre is complex and is beyond the scope of the present study. Also, to facilitate the analysis, the stress–strain curve of an unconstrained fibre is approximated by two straight lines (i.e. linear strain-hardening). To describe more realistic situations, more advanced studies will be needed.

Acknowledgements

The author thanks Drs P. F. Becher, J. M. Schneibel and E. Lara-Curzio for reviewing the manuscript. This research was sponsored by the US Department of Energy, Division of Materials Sciences, under contract DE-AC05-84OR21400 with Martin Marietta Energy Systems, Inc.

References

1. P. HING and G. W. GROVES, *J. Mater. Sci.* **1** (1972) 427.
2. V. V. KRISTIC, P. S. NICHOLSON and R. G. HOAGLAND, *J. Am. Ceram. Soc.* **64** (1981) 499.
3. D. HAN and J. J. MECHOLSKY, *J. Mater. Sci.* **25** (1990) 4949.
4. L. S. SIGL and H. E. EXNER, *Metall. Trans.* **18A** (1987) 1299.
5. F. ERDOGAN and P. F. JOSEPH, *J. Am. Ceram. Soc.* **72** (1989) 262.
6. H. E. DEVE, A. G. EVANS, G. R. ODETTE, R. MEHRABIAN, M. L. EMILIANI and R. J. HECHT, *Acta Metall. Mater* **38** (1990) 1491.
7. L. XIAO and R. ABBASCHIAN, *Mater. Sci. Eng.* **A155** (1992) 135.
8. T. C. LU, A. G. EVANS, R. J. HECHT and R. MEHRABIAN, *Acta Metall. Mater.* **39** (1991) 1853.
9. M. BANNISTER and M. F. ASHBY, *ibid.* **39** (1991) 2575.
10. M. F. ASHBY, F. J. BLUNT and M. BANNISTER, *ibid.* **37** (1989) 1847.
11. M. BANNISTER, H. SHERCLIFF, B. GAO, F. ZOK and M. F. ASHBY, *ibid.* **40** (1992) 1531.
12. J. BOWLING and G. W. GROVES, *J. Mater. Sci.* **14** (1979) 431.
13. *Idem, ibid.* **14** (1979) 443.
14. H. C. CAO, B. J. DALGLEISH, H. E. DEVE, C. ELLIOTT, A. G. EVANS, R. MEHRABIAN and G. R. ODETTE, *Acta Metall. Mater.* **37** (1989) 2969.
15. H. E. DEVE and M. J. MALONEY, *ibid.* **39** (1991) 2275.
16. H. L. COX, *Br. J. Appl. Phys.* **3** (1952) 72.
17. P. LAWRENCE, *J. Mater. Sci.* **7** (1972) 1.
18. A. TAKAKU and R. G. C. ARRIDGE, *J. Phys. D Appl. Phys.* **6** (1973) 2038.
19. M. R. PIGGOTT, "Load Bearing Fiber Composites" (Pergamon Press, Elmsford, NY, 1980) p. 62.
20. B. BUDIANSKY, J. W. HUTCHINSON and A. G. EVANS, *J. Mech. Phys. Solids* **34** (1986) 167.
21. Y. C. GAO, Y. W. MAI and B. COTTERELL, *J. Appl. Math. Phys. (ZAMP)* **39** (1988) 550.
22. D. K. SHETTY, *J. Am. Ceram. Soc.* **71** (1988) C107.
23. R. J. KERANS and T. A. PARTHASARATHY, *ibid.* **74** (1991) 1585.
24. C. H. HSUEH, *Mater. Sci. Eng.* **A125** (1990) 67.
25. *Idem, ibid.* **A154** (1992) 125.
26. P. A. MATAGA, *Acta Metall.* **37** (1989) 3349.
27. W. C. CARTER, E. P. BUTLER and E. R. FULLER Jr, *Scripta Metall. Mater.* **25** (1991) 579.
28. P. D. JERO and R. J. KERANS, *ibid.* **24** (1990) 2315.
29. T. J. MACKIN, P. D. WARREN and A. G. EVANS, *Acta Metall. Mater.* **40** (1992) 1251.
30. J. P. OUTWATER and M. C. MURPHY, in "Proceedings of the 24th Annual Technical Conference of Reinforced Plastic Composites Division", (The Society of the Plastics Industry Inc., New York, 1969) p. 11c.
31. J. W. HUTCHINSON and H. M. JENSEN, *Mech. Mater.* **9** (1990) 139.
32. C. H. HSUEH, *Mater. Sci. Eng.* **A145** (1990) 135.
33. C. H. HSUEH, *Mater. Sci. Eng.* **A123** (1990) 1.
34. R. HILL, "The Mathematical Theory of Plasticity" (Clarendon Press, Oxford, 1950).
35. C. H. HSUEH and A. G. EVANS, *J. Am. Ceram. Soc.* **68** (1985) 120.
36. C. H. HSUEH and P. F. BECHER, *ibid.* **71** (1988) C438.

Received 6 April
and accepted 16 June 1993